Thin Solid Films 519 (2011) 2362–2365

Contents lists available at ScienceDirect

Thin Solid Films

journal homepage: www.elsevier.com/locate/tsf

Magnetotransport properties of thin C–Fe films

J.C. Prestigiacomo [a], K.L. Lusker [b], Y.M. Xiong [a], S. Stadler [a], A.B. Karki [a], D.P. Young [a], J.C. Garno [b], P.W. Adams [a,*]

[a] Department of Physics and Astronomy, Louisiana State University, Baton Rouge, LA, 70803, USA
[b] Department of Chemistry, Louisiana State University, Baton Rouge, LA, 70803, USA

ARTICLE INFO

Article history:
Received 10 November 2009
Received in revised form 13 October 2010
Accepted 29 October 2010
Available online 4 November 2010

Keywords:
Magnetic thin films
Anomalous Hall effect
Iron carbide

ABSTRACT

The magnetotransport properties of C–Fe films formed by e-beam vapor deposition onto glass substrates are presented in the temperature region of 2 K to 300 K. Hall effect measurements reveal a significant anomalous Hall voltage whose magnitude increases with increasing temperature. Measurements of the ordinary Hall coefficient in 10 nm-thick films reveal a charge carrier density ranging from $n \cong 3.0 \times 10^{29}\ m^{-3}$ at 2 K to approximately half that value at 290 K. A comparison between anomalous Hall effect and parallel field magneto-optic Kerr effect measurements reveals a highly anisotropic coercive field with the easy direction lying in the plane of the film. Magnetoresistance measurements show that the films posses isotropic linear positive magnetoresistance beyond their saturation magnetization. The presence of carbon nanotubes formed during the e-beam process is confirmed via atomic force microscopy.

1. Introduction

Carbon–iron has a complex and technologically important binary phase diagram which includes iron allotropes, free graphite, and metastable iron carbide CFe_3 [1]. In practice, varying compositions of metastable phases can be trapped via non-equilibrium processes such as quench-condensation. Of these, cementite, CFe_3, has received the most attention. Although its mechanical, electrical, and magnetic properties have been studied for years, it has only recently been synthesized in bulk form [2,3]. Efforts to form CFe_3 films have included electron shower plasma vapor deposition [4], plasma enhanced chemical vapor deposition [5], and glow discharge methods [6]; in all cases the resulting film structure, morphology, and composition were found to depend dramatically on substrate temperature during deposition. These studies are motivated by the fact that metal-C films can be used as coatings to improve the strength, hardness, and wear properties of their pure metal counterparts [7]. In the present paper we present the magnetotransport properties of thin amorphous C–Fe films formed by e-beam vacuum deposition of arc-melted buttons of CFe_3 onto cryogenic substrates.

2. Sample preparation

C–Fe films of thickness 5, 10, and 20 nm were deposited onto liquid nitrogen cooled, fire polished silica glass substrates in a 0.4-μTorr vacuum by direct e-beam deposition of arc-melted C–Fe buttons. The buttons were synthesized from high purity graphite and iron with a starting stoichiometry of $CFe_{3.25}$ to account for some evaporative loss of Fe during the arc-melting process. The binary phase diagram of the carbon–iron system shows that the only intermetallic compound that will form from a mixture with 6.67% or more carbon by mass will be CFe_3, and that any excess carbon in the hypereutectic mixture will be precipitated out as graphite. However, due to the metastable nature of CFe_3 and the sensitivity of C–Fe alloys to cooling rates, one is not guaranteed to yield a single phase of this material. The upper curve of Fig. 1 shows the x-ray diffraction (XRD) pattern of the button used to deposit our films while the lower one represents the pattern of a resulting 100 nm film. From the pattern of the film we can see that it is amorphous but also retains some structure which is reminiscent of the Fe (110) plane. Patterns of the films used in our magnetotransport study were too thin to obtain an XRD pattern. Further XRD analysis of a pure 100 nm Fe film (not shown here) revealed an identical pattern to the C–Fe film. This implies that C is primarily in the form of an amorphous matrix, or has precipitated from the film in another manner. This latter possibility will be addressed later.

Hall and magnetoresistance measurements were performed using a standard 4-probe configuration with a Quantum Designs PPMS. The samples were tested at temperatures from 2 K to 290 K and in applied magnetic fields ranging from −9 T to 9 T. Coercive field measurements of 10 nm-thick ferromagnetic C–Fe and Fe films were taken at room temperature 30 min after deposition using the magneto-optical Kerr effect (MOKE) and then re-measured after exposure in air for 144 h for comparison. Ambient atomic force microscopy (AFM)

* Corresponding author.
E-mail address: adams@phys.lsu.edu (P.W. Adams).

0040-6090/$ – see front matter © 2010 Elsevier B.V. All rights reserved.
doi:10.1016/j.tsf.2010.10.066

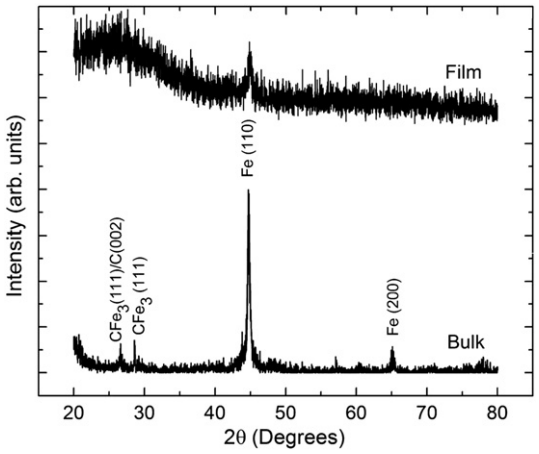

Fig. 1. XRD patterns of a 100 nm film (upper curve) and of the target button (lower curve).

characterizations were performed using tapping mode with an Agilent 5500 SPM equipped with PicoScan v5.3.3. Oxide-sharpened silicon nitride cantilevers from Nanosensors were used for imaging, with an average force constant of 48 N/m and a resonance frequency of 190 kHz.

3. Results and discussion

In the upper inset of Fig. 2 we show an AFM micrograph of a 5 nm thick C–Fe film that was deposited onto fire-polished glass at 84 K. The synthesis of thin films of metastable carbides CT_3 (T = Ni, Co) has been previously shown to form freestanding, vertical, multiwall carbon nanotubes (MWCNT) [8]. The synthesis of the C–Fe films presented here followed the same procedure as those experiments. The inset of Fig. 1 shows an AFM image of a 5-nm thick film which possesses many spike-like protrusions approximately 70 nm tall standing vertically out of the relatively smooth film matrix. Although we have not made a structural analysis of the protrusions, we believed that they are MWCNT or at least carbon "towers" that have precipitated out during deposition. Topography images were also acquired for 10 and 20 nm films; these too exhibit carbon spikes, although they were not as sharp as those in the 5-nm film. The mechanism by which the nanotubes nucleate and grow during the deposition is unknown [8]. However, the density of the nanotubes is too low to significantly affect the transport properties of the films.

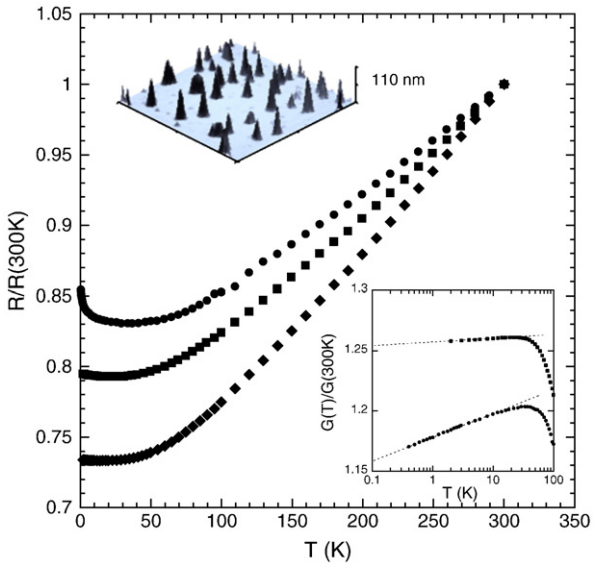

Fig. 2. Normalized sheet resistance of a 5, 10, and 20 nm thick C–Fe film as a function of temperature. The upper inset shows a 10 μm × 10 μm AFM image of the surface of a 5 nm-thick film. The spike structures are multiwall carbon nanotubes that are formed from carbon precipitating out of the C–Fe base. The lower inset shows the low-temperature logarithmic temperature dependence of the conductance of the 5 nm and 10 nm C–Fe films.

The temperature dependence of the resistivity of a 5, 10, and 20 nm-thick C–Fe film is shown in the main panel of Fig. 1. The resistivities have been normalized by their 300 K values. The films exhibit behavior typical of weakly disordered two-dimensional metals, with the resistivity decreasing with decreasing temperature until reaching a minimum near 20–30 K. Below this minimum the conductivity of the films decreases logarithmically, as can be seen in the lower inset of Fig. 1. This behavior has been observed in a wide variety of disordered thin film systems [9], and can be attributed to disorder-enhanced electron–electron interaction effects and/or coherent backscattering effects. Since the latter is usually suppressed in magnetic films, the anomalous logarithmic temperature dependence of the conductance in Fig. 1 is primarily due to electron–electron interactions.

The perpendicular magnetoresistance (MR) of a 10 nm film at 10 K is shown in the main panel of Fig. 3. The MR appears to have two components: a low-field contribution associated with the magnetization alignment, which saturates at about 1.5 T, and a rather weak linear contribution that extends to the highest fields studied. This linear positive magnetoresistance (LPMR) is also found in a parallel field configuration as shown in the inset of Fig. 3. The magnetization dependent component probably arises from spin scattering from magnetic moments in the film. The origin of the isotropic LPMR, however, cannot be explained by electron–electron interactions or the Lorentz force alone because they are expected to produce an MR that varies logarithmically or with the square field, respectively. Interestingly, LPMR has been reported in other C–Fe systems, but has not been adequately explained. In Fe_x–C_{1-x} composites this LPMR was observed to occur only at particular C–Fe ratios and temperatures [10]. The authors attributed the effect to competition between the Lorentz force in graphite and the deflection of charges around Fe nano-particles as their concentration was adjusted or the applied field was changed. Isotropic LPMR in ferromagnetic thin films of Fe, Ni, Co and their granular mixtures with other nonmagnetic materials has also been observed, and tentatively explained by a modification of quantum electron–electron interaction theory, though the results agree only

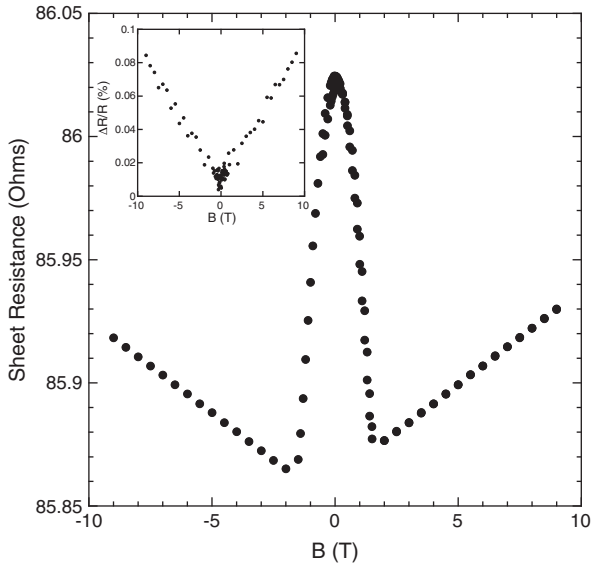

Fig. 3. Main panel: perpendicular magnetoresistance of a 10 nm-thick C–Fe film taken at 10 K. Inset: Parallel magnetoresistance of a 10 nm-thick C–Fe film taken at 2 K.

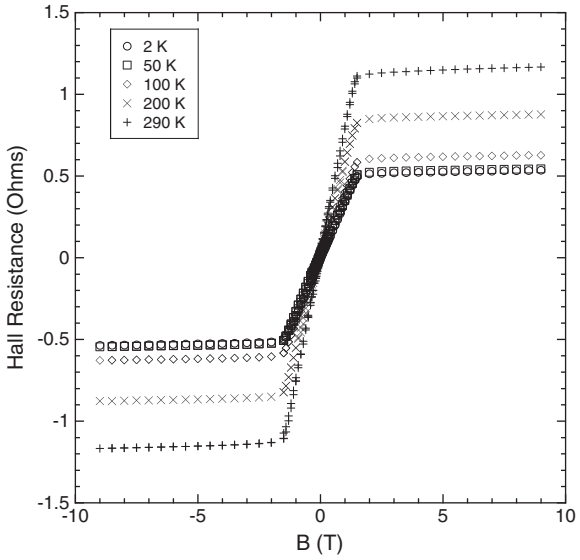

Fig. 4. Hall resistance of a 10 nm-thick film at a various temperatures. The steeply sloped low field region is due to the anomalous Hall effect. The ordinary Hall effect is represented by the much shallower slope of the high field regions (|B|>1.5 T).

qualitatively [11]. Our data is more consistent with this latter work, in that we observe a relatively robust, isotropic, LPMR.

The Hall resistance as a function of magnetic field is presented in Fig. 4 for selected values of temperature. The linear low field region, 0 to ~1.5 T, of the MR curve is due to the anomalous Hall effect (AHE) [12,13]. The knee in the curve represents the perpendicular saturation field of the magnetization. Beyond this saturation field the ordinary Hall effect produces a much smaller positive slope, from which the carrier density can be derived. Once the AHE contribution saturates, we can determine the ordinary Hall coefficient, $R_H = 1/ne$ by making a linear least-squares fit to the high field regions of the Hall resistivity curve, B>1.5 T and B<−1.5 T, in order to determine the slopes. The average of the negative and positive field slopes is proportional to R_H. Fig. 5 displays the temperature dependence of the Hall carrier density and we observe that the value falls from $n = 29.687 \times 10^{28}$ m^{-3} at 2 K to nearly half that value, $n = 15.995 \times 10^{28}$ m^{-3}, at 290 K.

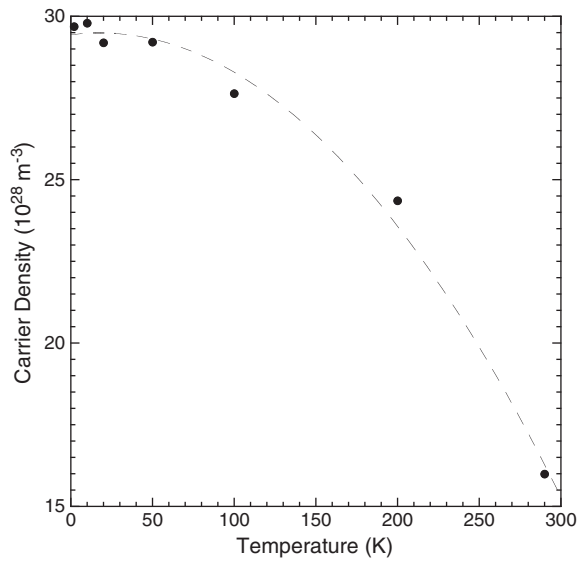

Fig. 5. Temperature dependence of the Hall carrier density. The dashed line represents a quadratic least-squares fit to the data.

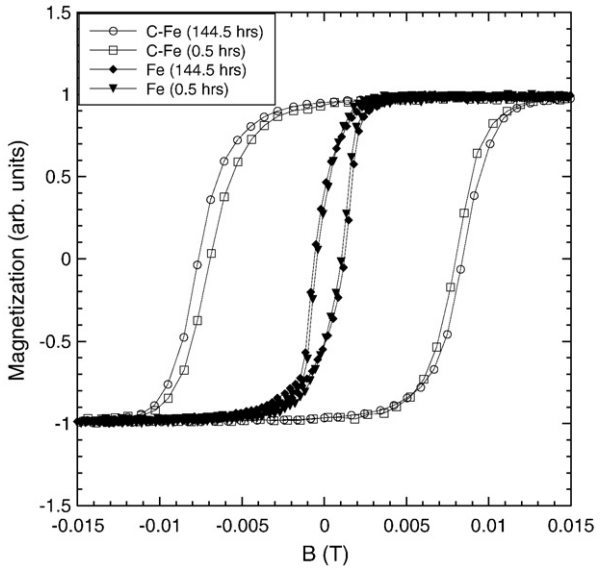

Fig. 6. Parallel field MOKE magnetization loops taken on a 10 nm-thick Fe film and a 10 nm-thick C–Fe film deposited under similar conditions. Data was taken immediately after the film depositions, and then the measurements were repeated 6 days later in order to document aging and/or oxidation effects. Note that the coercive field of the C–Fe film is approximately 5 times larger than that of the pure Fe film.

We have used longitudinal magneto-optical Kerr effect (MOKE) measurements to determine the in-plane magnetic properties of the C–Fe films. The coercive fields of 10 nm-thick Fe and C–Fe films with the field applied parallel to the film plane were determined at room temperature. As can be seen in Fig. 6, the parallel saturation fields are approximately 150 times smaller than their perpendicular counterparts as determined from AHE measurements, indicating an in-plane easy axis. This is expected for films of these thicknesses. Fig. 4 also shows the effects of oxidation on the coercive fields of an elemental Fe film and a C–Fe film. The hysteresis loops were measured after 0.5 h and 144.5 h of exposure to atmosphere. Clearly the coercive field rises over time; C–Fe increasing from ~69.2 Oe to ~76.4 Oe and Fe from ~4.5 to ~6 Oe. Although the coercive field of C–Fe is significantly

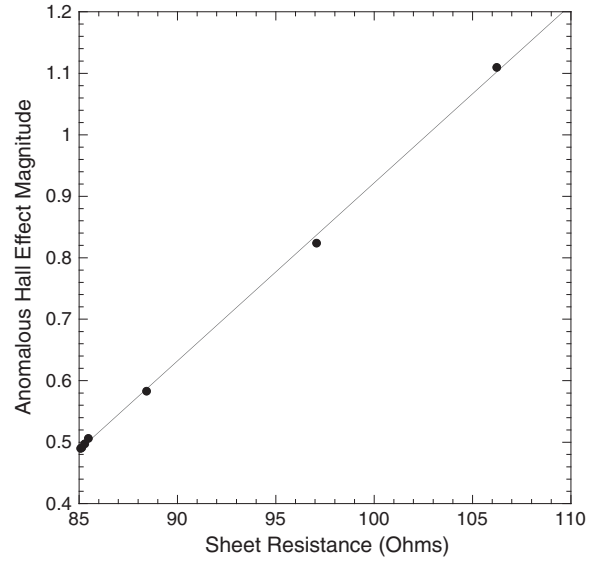

Fig. 7. Magnitude of the AHE as a function of the temperature dependent sheet resistance of a 10 nm-thick C–Fe film. The solid line is a linear least-squares fit to the data.

larger than that of pure iron, it is consistent with values obtained from getter sputtering onto ~200 °C quartz substrates [14].

We note that the magnitude of the AHE in Fig. 3 increases with increasing temperature. The total Hall resistivity is comprised of two terms [12,13],

$$\rho_H = R_o B + R_s M, \quad (1)$$

where R_o is the ordinary Hall coefficient, R_s is the anomalous Hall coefficient, and M is the magnetization. The saturation magnetization is expected to decrease with increasing temperature due to thermal fluctuations. Consequently, the magnitude of the AHE often decreases at higher temperatures. However, the anomalous Hall coefficient is itself a function of the longitudinal resistivity ρ. Since ρ varies with temperature, the AHE can also pick up a temperature dependence via R_s. Depending on the precise nature of the dominant scattering mechanism, R_s may be proportional to ρ or to ρ^2. The former corresponding to skew scattering and the latter to side-jump scattering [13]. In practice, R_s is often found to vary with ρ as a non-integer power between 1 and 2. In Fig. 7 we plot the AHE magnitude at each temperature against the sample's sheet resistance for that temperature. The data display a simple linear relationship between the two, suggesting that R_s is dominated by skew scattering, and that the temperature dependence of the AHE is primarily governed by R_s and not M.

4. Conclusion

In summary, we have presented electrical and magnetic transport properties of thin, metastable C–Fe films with thicknesses of 5, 10, and 20 nm. We observe a robust anomalous Hall effect that is dominated by skew scattering in this thickness range. Comparisons between the AHE saturation field and longitudinal saturation fields obtained from MOKE measurements show an anisotropic magnetization, with an in-plane easy axis. Magnetoresistance measurements show an isotropic linear positive magnetoresistance beyond the saturation magnetization which we believe is arising from electron–electron interaction effects. Further studies in C–Co and C–Ni films will be needed to verify the universality of the linear magnetoresistance. Topography images of the films provide clear evidence of multi-wall carbon nanotubes formed as an outgrowth of precipitated carbon during the deposition process.

Acknowledgements

P.W.A. acknowledges the support of the DOE under Grant No. DE-FG02-07ER46420. D.P.Y. acknowledges support from the NSF under Grant No. DMR- 0449022. J.C.G. acknowledges support from the NSF under Career: CHE-0847291. S.S. acknowledges support from the NSF under Grant No. DMR-0545728.

References

[1] G.J. Long, H.P. Leighly Jr., J. Chem. Ed. 59 (1982) 948.
[2] M. Umemoto, Z.G. Liu, H. Takaoka, M. Sawakami, K. Tsuchiya, K. Masuyama, Metall. Mater. Trans. A 32 (2001) 2127.
[3] H. Yumoto, Y. Nagamine, J. Nagahama, M. Shimotomai, Vacuum 65 (2002) 527.
[4] S.J. Li, M. Ishihara, H. Yumoto, T. Aizawa, M. Shimotomai, Thin Solid Films 316 (1998) 100.
[5] H. Siriwardane, O.A. Pringle, J.W. Newkirk, W.J. James, Thin Solid Films 287 (1996) 8.
[6] H. Siriwardane, O.A. Pringle, J.W. Newkirk, W.J. James, Thin Solid Films 279 (1996) 155.
[7] N. Laidani, L. Calliari, G. Speranza, V. Michcli, E. Galvanetto, Surf. Coat. Technol. 100–101 (1998) 116.
[8] D.P. Young, A.B. Karki, J.N. Ngunjiri, H. Zhu, B. Wei, D. Moldovan, J.C. Garno, P.W. Adams, J. Appl. Phys. 103 (2008) 053503.
[9] P.A. Lee, T.V. Ramakrishnan, Rev. Mod. Phys. 57 (1985) 287.
[10] Q.Z. Xue, X. Zhang, D.D. Zhu, J. Magn. Magn. Mater. 270 (2004) 397.
[11] A. Gerber, I. Kishon, I. Ya, Korenblit, O. Riss, A. Segal, M. Karpovski, Phys. Rev. Lett. 99 (2007) 027201.
[12] Gerd Bergmann, Fei Ye, Phys. Rev. Lett. 67 (1991) 735.
[13] S. Onoda, N. Sugimoto, N. Nagasoa, Phys. Rev. B 77 (2008) 165103.
[14] K. Watanabe, M. Munakata, K. Goto, Jpn. J. Appl. Phys. 26 (1987) L28.